

Implantation and Extraction of Penetrating Electrode Arrays in Minipig Retinas

Jinghua Chen¹, Vasiliki Poulaki², Seong-Joon Kim³, William D. Eldred⁴, Sheryl Kane⁵, Marcus Gingerich⁶, Douglas B. Shire⁶, Ralph Jensen², Gloria DeWalt⁴, Henry J. Kaplan⁷, and Joseph F. Rizzo, III⁸

¹ Department of Ophthalmology, University of Florida, College of Medicine, Gainesville, FL, USA

² Boston VA Healthcare System, Ophthalmology, Jamaica Plain, Boston, MA, USA

³ Department of Ophthalmology, Seoul National University College of Medicine, Seoul, Korea

⁴ Department of Biology, Boston University, Boston, MA, USA

⁵ Clean Membranes, Tyngsboro, MA, USA

⁶ Bionic Eye Technologies, Inc., Ithaca, NY, USA

⁷ Department of Ophthalmology and Visual Sciences, University of Louisville, Louisville, KY, USA

⁸ Department of Ophthalmology, Harvard Medical School and the Massachusetts Eye and Ear, Boston, MA, USA

Correspondence: Joseph F. Rizzo III, Neuro-Ophthalmology Service, Massachusetts Eye & Ear, 243 Charles St., Boston, MA 02114, USA. e-mail: joseph_rizzo@meei.harvard.edu

Received: September 3, 2018

Accepted: December 31, 2019

Published: April 24, 2020

Keywords: pillar array; penetrating electrodes; neural interface; retinal prosthesis; retinal implant; vitreoretinal surgery

Citation: Chen J, Poulaki V, Kim S-J, Eldred WD, Kane S, Gingerich M, Shire DB, Jensen R, DeWalt G, Kaplan HJ, Rizzo JF III. Implantation and extraction of penetrating electrode arrays in minipig retinas. *Trans Vis Sci Tech.* 2020;9(5):19, <https://doi.org/10.1167/tvst.9.5.19>

Purpose: This work was motivated by the goals of demonstrating methods to fabricate and implant large numbers of penetrating arrays into the retina and the feasibility of extraction.

Methods: Arrays of inactive, three-dimensional (3D) SU-8 structures were microfabricated onto 13- μm polyimide substrates. Standard vitreoretinal surgical techniques were used with an *ab externo* approach for subretinal implantation of arrays in 12 mini-pigs. In the first three surgeries, different post-geometries were explored, while a preferred design (128- μm tall, 30- μm diameter, 200- μm spacing) was used for the remaining nine implantations. Two arrays were extracted. Funduscopy, optical coherence tomography (OCT) and immunohistochemistry of the retinae were performed. The unoperated eyes and tissue far from implantation served as controls. A thirteenth pig was implanted with a planar array.

Results: Ten implant surgeries had no significant complication, and two arrays were successfully extracted. One retinal tear occurred after implantation due to too long posts in an early surgery. In "successful" cases, OCT showed close apposition of the arrays to the retina and integration of the posts, the tops of which were positioned at the junction of the inner plexiform and ganglion cells, without significant gliosis.

Conclusions: These results provide a proof-of-concept that relatively large numbers of 3D posts can be implanted into, and extracted from, the retina of mini-pigs. Our surgical numbers were relatively small, especially for the extractions, and our conclusions must be viewed with that limitation. Our methods are applicable for human surgeries.

Translational Relevance: This study provides results of implantation and extraction of relatively large numbers of 3D posts from the retina of minipig eyes. If similar technology were used in humans, a 3D array of this type should lower perceptual thresholds, provide safer long-term stimulation, and perhaps provide better perceptual outcomes.

Introduction

Visual prostheses are being developed by numerous groups around the world as a strategy to restore vision to patients affected by neural forms of blindness.^{1–20} Each of these approaches seeks to bypass damaged or dysfunctional nerve tissue to deliver visually relevant neural stimulation along surviving visual pathways.^{21–25}

The most significant challenge for any neurosensory prosthesis is achieving a biocompatible interface in which mechanical and electrochemical damage are minimized to increase the potential for psychophysical benefit. For a retinal prosthesis, there is the added challenge of the need to deliver a sufficiently large number of relatively small electrodes to enhance the perceptual quality.^{15,26–31} One dominant factor that influences the potential for highly focal activation of neurons is the distance between the stimulating electrode and the target neurons.^{32,33} For instance, in the dawn of visual cortical prosthetic research in humans, it was demonstrated that penetrating electrodes enabled lower perceptual thresholds and improved the quality of visual percepts compared with stimulation delivered through surface electrodes.^{4,13,16,24,34–38} At the level of the retina, we previously demonstrated that a separation of only 50 μm between the electrode and neurons increases the stimulation threshold 2.4- to 8-fold, depending on polarity.³⁹ Notably, electrodes positioned on either the epi- or subretinal surface will lie at least 30 μm from neurons that are the intended targets of stimulation, and thus would require higher stimulating charges. The only strategy to minimize stimulating current is to position the electrodes within the retinal neurons, which is challenging given the delicate nature of the retina.

Palanker et al.^{37,40} were the first to demonstrate that “penetrating” electrodes could be inserted into a rodent eye without significant tissue destruction. Our group extended this finding from the rodent into a minipig model⁴¹ by leveraging, and then modifying, surgical techniques that we had developed for planar arrays in rabbit eyes.⁸ As an extension of our earlier work, herein we describe methods to microfabricate a relatively large number of three-dimensional (3D), nonelectrically active posts on a thin, polyimide substrate and to implant these devices into the retinas of minipigs. Our specific goals were to define device-level factors that enable implantation of large numbers of small penetrating structures into the retina toward a future goal of human experiments that could potentially yield: (1) lower perceptual thresholds; (2) safer

long-term electrical stimulation; and (3) better perceptual outcomes than could likely be achieved with planar electrodes. Given our longer-term intention to incorporate 3D electrodes into a device for humans, we also sought to assess the biocompatibility of these arrays, especially because the posts have the potential to penetrate and disrupt the retina more than planar arrays.

Methods

The protocol for this research was approved by the animal care committees of the Massachusetts Institute of Technology (MIT) and the Veterans Administration Medical Center (VAMC), Jamaica Plain, Boston. All animals were treated in accordance with the Association for Research in Vision and Ophthalmology resolution on the use of animals in research and the principles of laboratory animal care. The fundamental surgical methods used in this study had been developed over many years and used to perform an earlier biocompatibility study with planar electrodes⁴² and later to remove planar electrode arrays from rabbit eyes.⁸ To then study the biocompatibility of penetrating electrodes, several additional years of work were required to modify our surgical methods to enable implantation of large numbers of penetrating structures into the minipig retina without inducing undue damage. The results reported herein represent the culmination of that earlier developmental work that was performed with a much larger number of pigs.

Animals

Twelve Yucatan minipigs consecutively underwent intraocular surgery to implant a 3D array into the subretinal space. All pigs were female, typically 4 to 6 months of age, with a range of weights from 18 to 25 kg. Two animals underwent surgery to extract the array months after implantation. One additional minipig was implanted with our earlier planar array to demonstrate the degree to which the retina thins in the area overlying the implant as a guide for the height of the 3D posts that would eventually be used.

Pillar Arrays

Electrically inactive, 3D “pillar” arrays were microfabricated at the Cornell NanoScale Science and Technology Facility. The substrate was made of polyimide, and the pillars were made of photocross-linked SU-8, which is a widely used, gener-

Table. Geometric Characteristics of Pillar Arrays

Pillar Version	Number of Eyes	Substrate Thickness (μm)	Range of Pillar Height (μm)	Range of Pillar Diameters (μm)	Range of Pillar Densities (μm)
Version 1	3	13 μm	70–128 μm	10–80 μm	50–300 μm
Version 2	9	13 μm	128 μm	30 μm	200 μm

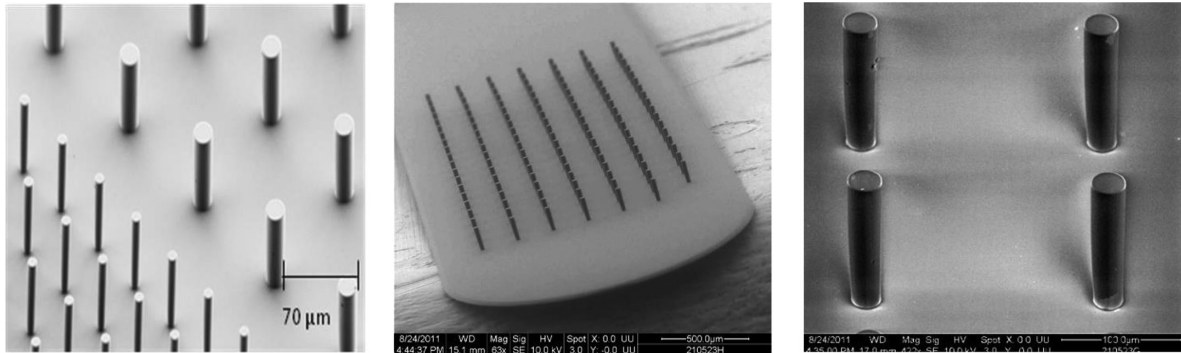


Figure 1. Scanning electron micrographs of two different 3D pillar arrays. The substrate was made of 13- μm thick polyimide; the pillars were made of cross-linked SU-8 epoxy. *Left:* Example of an early test pillar array that contains 295 pillars, showing two different types of geometries that differed in terms of pillar diameter (10 or 20 μm), and density. *Middle:* Preferred pillar array (63x magnification) used for most implant surgeries. This array contains 126 pillars, in which each has a 30- μm diameter and is 128- μm tall, with 200- μm center-to-center spacing, covering a total area of 1.2 mm \times 3.4 mm. *Right:* Magnified (422x) view of the preferred pillar array.

ally biocompatible, epoxy-based photoresist polymer. The polyimide was initially spun onto a silicon wafer and fully cured. Any outline shape of the polyimide substrate was then defined by contact lithography and reactive ion etching. SU-8 was finally spun on and the pillars were formed by ultraviolet exposure with a mask using contact lithography and wet chemical dissolution of the non-cross-linked material. Initially, a variety of pillar geometries (version 1) were used, with pillar heights ranging from 70 to 128 μm (Table; Fig. 1). After examining initial histological outcomes from three implants using version 1 arrays, we selected geometric features for version 2 (Table) for the last nine implants. For these latter surgeries, the polyimide foundation on which the pillars were constructed was 1.7-mm wide \times 15-mm long \times 13- μm thick, over which 126 pillars were distributed. This density of the pillars was chosen because of more well-preserved retinal architecture that was found compared with more dense geometries (results not reported here). The choice of pillar height was based on achieving a desired goal of postimplant positioning of the tip of the pillars roughly at the border between the inner plexiform layer (IPL) and the ganglion cell layer (GCL).

Coatings

The 12 arrays received surface modifications at EIC Laboratories (Norwood, MA) that included coating

with a \sim 1- μm thick layer of Parylene-C using a Specialty Coating Systems PDS 2010.⁴³ Both the monomer and coating equipment were obtained from Cookson Electronics (Indianapolis, IN).

Implantation Surgery

All surgeries were performed by the same surgeon (JC) between 2008 and 2013, either at MIT or the VAMC in surgical suites that were similarly equipped. Our detailed surgical methods have been previously published.⁸ In brief, for all surgeries anesthesia was induced with intramuscular injection of Telazol, Zoetis Inc. New Jersey (USA) (4 mg/kg) and xylazine (2.2 mg/kg) and maintained with 1% to 3% isoflurane inhalation. To avoid excessive bleeding during surgery, systemic hypotension (maintained at 45-50 mm Hg by monitoring with an intra-arterial line while infusing intravenous sodium nitroprusside 50 mg/250 mL) was used during insertion of the pillar array to reduce the risk of choroidal hemorrhage.

An ab externo surgical approach was used to enter the subretinal space via the superotemporal quadrant, 10 mm posterior to the limbus. A core vitrectomy was performed using a vitrector (The Millennium Bausch + Lomb, Inc., Rochester, NY), and a local retinal detachment (i.e., “bleb”) was created by injecting balanced salt solution via a Lambert cannula, followed by injection of Healon (Johnson & Johnson, New Brunswick, NJ)

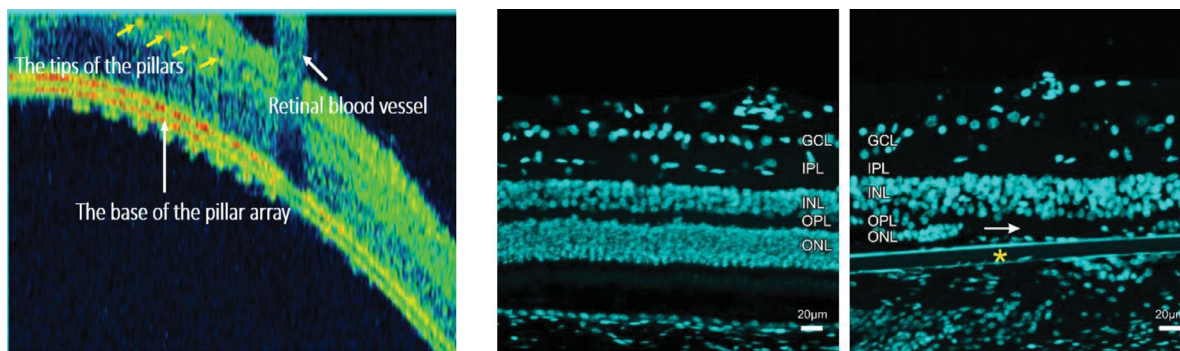


Figure 2. Surgical implantation of a subretinal electrode array substrate in a pig. *Left:* OCT of a subretinal electrode array 1 month after surgery. Typically, implantations include a 7- to 8-mm length of substrate material, the distal end of which contains electrodes distributed over a 2-mm² area (although with some variation among different array designs). This OCT image reveals that the array achieves close and conformal apposition to the retina (here shown over a 2.2-mm segment) without the use of a tack or adhesive. *Middle and Right:* Histology of pig retina with immunohistochemical staining with DAPI that highlights neuronal cell bodies. *Middle:* Control retina showing the three nuclear layers: ONL, inner nuclear layer, and GCL. *Right:* One month after implantation of a planar polyimide strip (yellow asterisk) without 3D features into the subretinal space. The ONL is substantially reduced in thickness. There were reduced number of nuclei in ONL and disorganization of the cells. The white arrow shows the space was occupied by nuclei. The preferred height of the pillar arrays was based on consideration of the degree of retinal thinning that occurs because of subretinal placement of the electrode array and on the desire to position the tip of the pillars within, or at least near to, the IPL.

through the retinotomy. A scleral flap was made behind the area of the retina that was intended for implantation. After cauterizing the uveal tissue exposed by the flap, a polyimide “guide” (2 mm x 10 mm x 75 μm) and overlying pillar array were simultaneously introduced through an incision made into the uvea to reach the subretinal space; the guide was retracted just after the insertion was complete. The proximal, extrascleral length of the polyimide strip was fixed to the sclera (with sutures passed through customized eyelet holes), and the scleral flap was closed with 7-0 Vicryl sutures. Figure 2 left shows an optical coherence tomography (OCT) image of the conformal alignment of the 3D array to the subretinal surface. Figure 2 right shows the degree of degeneration of the outer nuclear layer (ONL) that occurs in the area overlying a planar array.

Explantation Surgery

Removal of the array was performed in two animals. In the first animal, the array was extracted 3 months after implantation, after which the animal was immediately euthanized. In the second animal, the array was extracted 2 months after implantation, then the animal survived for another month so that the subsequent histological analysis of the retina and eye could assess the degree to which the extraction surgery might have initiated inflammatory/fibrotic reactions. After anesthetizing the animal as described earlier, the initial step to remove the arrays involved resection with scissors and forceps of the small amount of fibrotic

tissue that had formed on the posterior scleral surface around the site at which the array had been inserted into the eye. Then, the retina was separated from the array by gently injecting balanced salt solution above and below the polyimide cable via the ab externo entry site that had been used to implant the electrode array. After extraction, the scleral slit was closed with sutures.

Examination Protocol

Clinical examinations and fundus photographs were performed presurgery, at 1 week, and each month thereafter postsurgery. In vivo images of the implanted pillar arrays were obtained with a fundus camera and with OCT (Zeiss Cirrus HD-OCT Version 3.0, Carl Zeiss Meditec AG Göschwitzer Straße 51-52 07745 Jena, Germany). The animals were followed 1 to 8 months after surgery; at the end of the specified survival time, the animals were euthanized, and the eyes were enucleated and prepared for histology.

Histological Preparation

The anterior segment, lens, and vitreous were removed, leaving a posterior eyecup that contained the sclera, choroid, retinal pigment epithelium (RPE), and neural retina. The location of the extracted implants was confirmed by gross observation and by comparison to fundus photographs, and the orientation to the implanted area was marked by a suture

to assure that histological slides were made immediately adjacent to the area where the array had been implanted and extracted. The eyecups were fixed with 4% paraformaldehyde in phosphate buffer (PB) for 2 hours, then cryoprotected using a sucrose gradient (5%–30%), embedded in Optimal Cutting Temperature media (Tissue-Tek, Miles, Inc., Elkhart, IN), frozen, then cut with a cryostat into 25- μ m thick sections that were collected on Superfrost Plus slides (Fisher Scientific, Waltham, MA). Sections were stored at -20°C before being used for immunocytochemistry.

Histological Staining and Immunohistochemistry

DAPI (4',6-diamidino-2-phenylindole) was used to stain nuclei of cells, including especially retinal neurons. Immunohistochemical staining was used to define specific cell types or elements. For instance, rabbit polyclonal anti-glial fibrillary acidic protein (GFAP; Cat# ab 7260, Abcam, Cambridge, MA, 1:32K) and mouse monoclonal anti-GFAP (Cat# 3670, Cell Signaling Technology, Danvers, MA) were used to identify Müller cells and gliotic reactions; mouse monoclonal anti-pig CD45 was used to label activated microglia (Cat# MCA1222G, AbD Serotec, Raleigh, NC); and mouse monoclonal anti-synaptotagmin (Cat# mAb 30(asv30) developed by Louis Reichardt and obtained from the Developmental Studies Hybridoma Bank developed under the auspices of the Eunice Kennedy Shriver National Institute of Child Health and Human Development [NICHD] and maintained by the University of Iowa, Department of Biology, Iowa City, IA) was used to label neuronal synaptic vesicles.

For conventional bright-field immunocytochemistry, the sections were processed using standard procedures as recommended by the Vectastain ABC-Elite kit for mouse or rabbit IgG (Vector Laboratories, Burlingame, CA). In brief, sections were thawed at 37°C , rinsed in PB, and incubated in either 1.5% normal donkey blocking serum (Cat# 017-000-121, Jackson ImmunoResearch Labs, West Grove, PA) or normal goat blocking serum (Cat# 005-000-121, Jackson ImmunoResearch Labs) in PB for 4 hours at room temperature. Sections were then incubated in primary antiserum overnight, rinsed in PB, incubated in biotinylated secondary antiserum for 1 hour, and then in avidin-biotin reagent for 1 hour. Labeling was visualized with 3, 3' diaminobenzidine and H_2O_2 (DAB kit, Vector Laboratories). Control sections were not exposed to primary antibodies, but otherwise were processed similarly through all other steps.

For confocal immunocytochemistry, the tissue sections on slides were washed with PB to remove excess optimal cutting temperature media. All antiserum solutions were diluted in PB with 0.3% Triton X-100 (PBtx). Nonspecific labeling was blocked by incubation in 5% normal donkey serum (Cat# 017-000-121, Jackson ImmunoResearch Labs) in PB for 1 hour. Sections were then incubated in primary antiserum overnight at 4°C . Following incubation in primary antiserum, the sections were washed in PB and incubated for 2 hours in the appropriate PB diluted (1:500) fluorescent secondary antisera, either Alexa 488-conjugated donkey anti-rabbit IgG, (Cat# A-11008, Molecular Probes, Carlsbad, CA) or DyLight 649-conjugated donkey anti-mouse IgG (Cat# 715-495-150, Jackson ImmunoResearch Labs). To control for nonspecific secondary antiserum staining, some slides were incubated in normal serum without primary antiserum before the secondary antiserum was applied. The slides were then washed in PB and cover-slipped with glycerol and examined using a FluoviewTM 300 confocal microscope (Olympus Corporation, Melville, NY) with a 40x oil immersion objective with a numerical aperture of 1.00. In some cases, DAPI was added to the glycerol cover slip solution to label all nuclei. For double-labeling experiments, each secondary antiserum was excited by a different laser wavelength (either 488 or 647 nm). As a control for double labeling, each primary antiserum was paired with the opposite secondary antiserum. The stacks of 12 to 14, 1- μ m thick optical sections were collected, collapsed, and converted to 8-bit grayscale images using Image J software (Wayne Rasband, National Institute of Mental Health, Bethesda, MD), and then imported into Corel Draw 14 (Corel Corporation, Ottawa, Canada) for brightness and contrast adjustment, arrangement, and labeling.

Results

Clinical Examination

Twelve consecutive surgeries succeeded in implanting the pillar arrays into the subretinal space. Ten of the 12 surgeries were considered successful in that the implant was inserted into subretinal space or extracted without obvious surgical or postoperative complications, including significant behavioral change in the animal, clinically detectable inflammation or infection, significant hemorrhage, cataract, retinal tear, retinal detachment, tissue incarceration, hypotony, proliferative vitreoretinopathy, or other untoward event that could be construed as potentially threatening the health

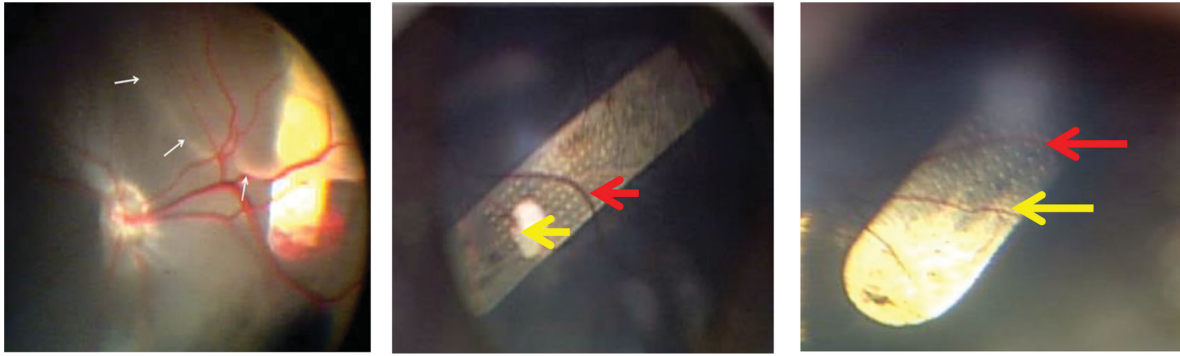


Figure 3. Fundusoscopic photographs taken at different times of the same 3D electrode array implanted into the subretinal space of a minipig. *Left:* Intraoperative appearance just after insertion of the pillar array. The *white arrows* demarcate the edge of the retinal bleb that was made to facilitate introduction of the array. A small hemorrhage is evident under the retina but above the array; this hemorrhage cleared spontaneously within weeks. *Middle:* One month after implantation, there is seemingly good apposition between the array and the retina, without obvious gliosis. The *red* and *yellow arrows* highlight two retinal blood vessels; the *white area* under the *yellow arrow* is a reflection of light from the operating microscope. The penetrating posts can be recognized as small, white dots that appear in an organized pattern across the polyimide strip (*bronze colored structure*). *Right:* Two months after surgery, there continues to be a clear and even view of the implant through the retina. The *red* and *yellow arrows* highlight the same two vessels shown in the *middle* photograph. Although reflection artifacts detract from the quality of the view, no obvious gliosis was identified clinically, and the retina appeared attached, with seemingly well-integrated 3D posts. Although challenging to appreciate in the *right* photograph because of reflections, the location of the array had not shifted, as can be judged by the consistent presence of seven rows of posts above the upper margin of the vessel highlighted by the *red arrow* in the *middle* and *right* photographs.

of the eye, retina, or animal. Signs of postoperative inflammation that were assessed included persistent conjunctival injection, chemosis, and anterior chamber reaction. Two surgeries were considered to have failed because of fibrotic responses in the region of the implant that were perhaps incited by intraocular hemorrhage. One initially catalogued as successful surgery was complicated by a retinal detachment 14 weeks after implantation; the cause of the detachment was penetration of the inner retina by the relatively long posts that were used in the earlier surgeries. Our earlier surgeries, and the result from one animal included herein that had been implanted with a planar array (Fig. 2, right), confirmed the expected thinning of the retina overlying the implant, which occurs because of degeneration of the outer retina, presumably owing to blockage of nourishment from the choroid. The degree of thinning varies somewhat among animals, and our failed surgical outcome guided refinement of a preferred length of the posts (to reach the boundary of the inner plexiform and GCLs) for subsequent implants, and no other retinal detachments occurred thereafter. In the other nine successful cases, the 3D posts penetrated the retina in a seemingly uniform pattern across the array (Fig. 3).

Optical Coherence Imaging

Serial postoperative OCT examinations revealed gradual resolution of subretinal fluid and gradual

integration of the pillars into the retina (Fig. 4). This imaging also revealed that the subretinal substrate was in contact with and conformal to the retina, which enabled an even insertion of the posts up to the same retinal depth.

On some OCT images, the pillars did not appear to be perpendicular to the base. This appearance is likely the result of two factors: (1) the darkness seen on the OCT image is not the post itself, but rather the shadow of the post, as the incoming light from the OCT is blocked by the tip of the post; and (2) the OCT scans may not perfectly align vertically over the row of pillars. This explanation is made evident in the OCT image of Figure 4, which shows only four posts even though there were seven pillars in each row (i.e., it missed the two left-most pillars and the one furthest to the right). The misalignment also accounts for the relatively thin shadow of the upper part of the left-most post, and the wider than typical base of the second post from the left.

Immunocytochemistry

Figure 5 shows a magnified image of a single, 128- μm tall pillar that integrated into the retina and reached our target location, that is, the border between the inner plexiform and GCLs. This pillar height was then used for the subsequent surgeries. Figure 5 left also shows a band of neuronal synapses (imaged by labeling synaptic vesicles) within the IPL draped

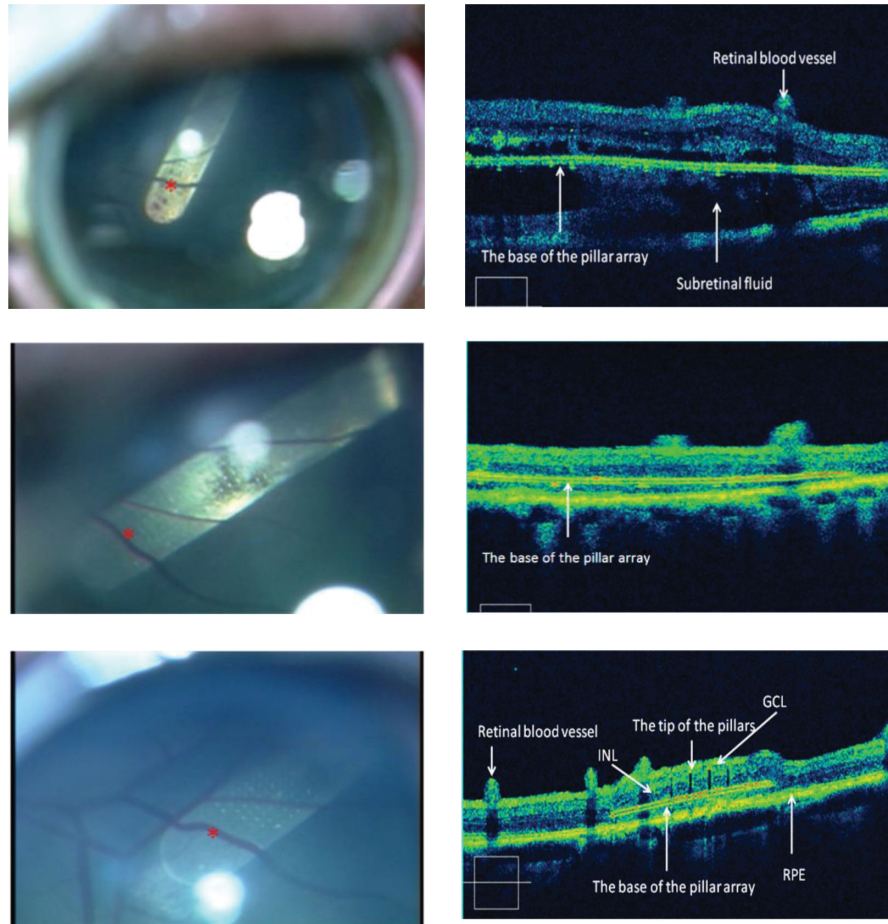


Figure 4. Fundus photographs (*left*) and OCT images of the retina (*right*) taken at different times in one minipig (different from the pig shown in Fig. 2). The *upper*, *middle*, and *lower* rows show images obtained 1 week, 1 month, and 2 months postimplantation. The *red asterisks* shown on the fundus photographs each highlight the same blood vessel. *Upper row*: OCT revealed subretinal fluid and fluid between the array and retina that were not evident by clinical examination. *Middle row*: At 1 month, the retina is fully attached, and there is no subretinal fluid, however, integration of the pillars cannot be visualized. *Lower row*: At 2 months, the retina remains fully attached, and there is no subretinal fluid. The subretinal substrate is in contact with and conformally aligned with the retina, and the pillars evenly penetrate the retina up to the junction of the inner plexiform and retinal GCLs. Optical shadows are evident beneath blood vessels, and the tips of the pillars can be seen (but not the pillar shafts themselves). INL, inner nuclear layer.

around the tip of the posts, which will be the site at which electrical stimulation will be delivered in future experiments. Figure 5 middle further demonstrates even positioning of pillars, with 200- μm center-center spacing, into the retina.

Figure 5 middle and right also demonstrates glial responses to the implantation of pillars into the retina. For instance, GFAP staining (middle image) highlights Müller cells and astrocytes. Staining of this degree is regularly observed over a wide field after essentially any manipulation of the retina, and certainly after inducing a retinal detachment, which is a preliminary step in our implantation procedure. The CD45 antibody, which labelled activated microglia (Fig. 5, right), demonstrated reaction only along the shaft of the pillar. Although some gliosis was found around the

array in all specimens, in no case was there significant gliosis at the top of the posts, where electrical stimulation will eventually be delivered, nor were any posts encapsulated.

The images of the pillars that showed tilting with respect to the base (for instance, Fig. 5, left) are the result of the histological processing of the tissue, which requires freezing and cutting of the tissue and array with a cryostat. By contrast, the unprocessed *in vivo* tissue with perpendicularly oriented posts can be seen in the OCT images of the same figure.

Explantation Surgery

Extraction of the electrode array was performed without difficulty in 2 animals 2 and 3 months



Figure 5. Immunohistochemical staining (transverse section) of pig retina 1 month following subretinal implantation of a 3D array. *Left:* Single pillar (red asterisk; 128- μ m tall; 30- μ m diameter) extending from the polyimide substrate (yellow asterisk) to the top of the IPL (red arrow), just below the retinal GCL (white arrow). Nuclei are labeled with DAPI. Synaptic vesicles (a proxy for synapses) are labeled with synaptotagmin (Mab30, green). The tip of the pillar electrode, which is the site at which electrical stimulation will be delivered in the future, is capped by neuronal synapses at the upper aspect of the IPL. Inner nuclear layer (white arrowhead); ONL (red arrowhead); epi-retinal surface (yellow arrow). Magnification: 60x. Scale bar: 30 μ m. *Middle:* Lower magnification (10x) view of the retina from the same pig showing the position of three consecutive pillars (center pillar: red asterisk) with 200- μ m center-center spacing. The tip of each post rests at the upper border of the IPL in red with Mab30. Glial acidic fibrillary protein (green) was used to label Müller cells and astrocytes. Nuclei are labeled with DAPI (blue). Scale bar: 100 μ m. GCL: ganglion cell layer; INL: inner nuclear layer; OPL: outer plexiform layer. *Right:* Immunohistochemical staining (transverse section) of same pig retina shown in Fig. 5 1 month following subretinal implantation of 3D arrays. Mouse monoclonal anti-pig CD 45 (red) was used to label activated microglia. Glial acidic fibrillary protein (green) was used to label Müller cell bodies and astrocytes. The yellow arrow shows the tip of a single pillar (white asterisk). There are some activated microglial cells along the sides of the pillar and mild general upregulation of GFAP staining of the Müller cells and astrocytes, but the tip of the pillar did not elicit a prominent glial response. Magnification 60x. Scale bar: 25 μ m. GCL, ganglion cell layer; INL, inner nuclear layer; OPL, outer plexiform layer.

postimplantation, respectively. In one case, the array was extracted without any detectable resistance; in the other case, there was some resistance to extraction, which was relieved by a second transretinal injection of balanced salt solution to further elevate the retinal bleb under fundusoscopic guidance. Then, at the scleral opening, forceps were used to gently retract the array, without need for additional dissection of tissue. In neither case was there detectable damage to the retina after the explanation, at least as could be judged with high magnification fundusoscopic viewing during surgery.

Retinal histology was performed in both extraction cases. In one case, the animal was euthanized immediately after the extraction, whereas the other animal was euthanized 1 month after extraction of the array. This dual approach provided a comparative assessment of retinal damage that might have occurred secondary to the implant itself versus the surgical extraction of the implant. In the latter case, biological responses might have been initiated by the extraction that would have been missed in the animal that had been euthanized immediately after the extraction.

Figure 6 shows the results obtained 1 month after extraction compared with retina from the same animal taken at a substantial distance from the implanta-

tion/extraction site. The two images, which were taken at the same magnification (i.e., 60x), show that the site of implantation/extraction is thinner than the “control” site. The reduced total thickness is primarily the result of a thinner ONL, which is not unexpected given that our array was placed in the subretinal space (where it blocked choroidal nutrients to the retina). This retina also shows slightly more gliosis than the control. There is no other gross or other discernible change to the integrity of the tissue. The lack of visual evidence of where the posts had been positioned is probably the result of tissue remodeling after the posts had been extracted. We note with interest that the thickness of the ONL in Figure 6, right, although decreased compared with the control image in the same figure, is thicker than that shown in Figure 5. This intermediate thickness of the ONL 1 month after explanation could plausibly be the result of repopulation of neurons in this area. There is evidence from the work of others that regrowth of ONL neurons can occur in experiments in which there is chronic disruption of the boundary between the outer retina and RPE, especially in the context of a subretinal implant. We conjectured that repopulation of neurons, if indeed this had occurred, might have been induced by upregulation and release of a diffusible growth factor.⁴⁴

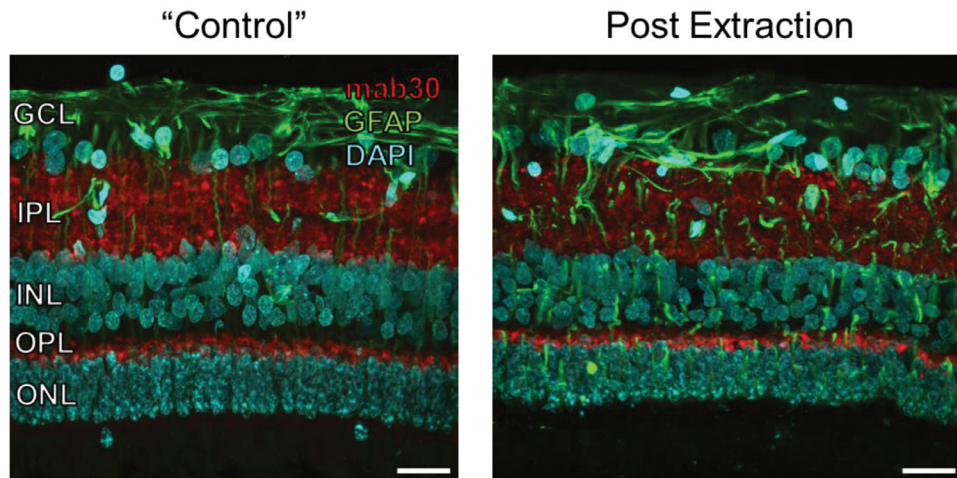


Figure 6. Immunohistochemical staining (transverse section) of the same pig retina, far away from (left, “Control”) and immediately adjacent to (within 100–200 microns) the site of implantation, then extraction (right) of a 3D electrode array. The array had been implanted for 2 months, followed by a 1-month survival period. The nuclei of retinal neurons are highlighted by staining with DAPI (blue); neuronal synaptic vesicles in both plexiform layers are highlighted with the Mab30 (red) antibody; GFAP (green) highlights Müller cell bodies and astrocytes. There is no obvious difference in appearance between the extracted and control retina, indicating that the process of extraction did not cause any discernible damage immediately adjacent to the site of implantation, at least as can be judged by these methods. Magnification: 60x for both images. Magnification: 60x for both images. Scale bar: 50 μ m. GCL, ganglion cell layer; INL, inner nuclear layer; OPL, outer plexiform layer.

Discussion

Specific goals of this work included defining device-level factors that would enable implantation of large numbers of penetrating structures into the retina of minipigs. We also sought to assess the biocompatibility of our 3D arrays, especially because the posts have the potential to penetrate and disrupt the retina more than planar arrays. To achieve these goals, we developed methods to microfabricate 3D structures on an ultrathin and biocompatible substrate and to surgically implant the devices into the subretinal space, which is our intended site of electrical stimulation in future human experiments. Our interest in working with 3D arrays was driven by our earlier findings that proximity of the stimulating electrode (which, in our design, will be at the tip of the posts) to retinal neurons would lower activation thresholds of the neurons.^{26,45} Lower activation thresholds also would lower the stimulating charge densities, which should improve biocompatibility of the device and the survivability of the electrodes.^{37,39,40,46–52}

Nonelectrically active posts were used to conduct this anatomic assessment of the effects of surgery and the biological reactions to the implant itself, and in some cases, extraction of the implant. Implantation and explantation of epi- and subretinal planar electrode arrays have been demonstrated by others.^{5,7,17} However, implantation and explana-

tion of relatively tall posts able to reach the inner retina has not been shown before. The dummy 3D posts used in this study did not contain metals to deliver electrical impulses. The inclusion of metals will slightly stiffen the arrays, which might require fine adjustments in maneuvering the array into the eye. The increased stiffness also will to some extent promote rectification of the curvature of the array once it is in the subretinal space. The potential impact of these factors will be assessed in other *in vivo* experiments.

Our study demonstrated that: (1) a relatively large number of 3D posts could be implanted into the retina while maintaining the general integrity of the retina, save for the expected loss of the ONL (which occurs with chronic placement of a subretinal membrane, as discussed later); (2) relatively large numbers of 3D posts can be positioned within the retina and provide minimal physical separation between tip of the pillars and neurons or neuronal; (3) conformal alignment and similar depth of penetration of the 3D posts can be achieved over the length of the array; (4) stable positioning of the array of posts over a period of up to 8 months can be achieved without use of tacks or adhesive; (5) penetration of posts into the retina can be performed without inducing significant gliosis; and (6) a thin film substrate with 3D posts can be extracted from the retina and eye months after implantation without causing significant damage. All of our

specimens showed degeneration of the outer retina, which was expected to occur.

The pig retina, like the human retina, has a dual (i.e., retinal and choroidal) blood supply, and a subretinal implant blocks diffusion of oxygen and metabolic transfer between the outer one-third of the retina and the underlying RPE. This outcome is acceptable for this experimental model because the pattern of anatomic degeneration is grossly similar to blinding diseases that we are attempting to treat, namely retinitis pigmentosa (RP) and macular degeneration (it is not known, however, if this type of induced retinal degeneration includes the well-established patterns of “retinal remodeling” that Marc so convincingly demonstrated in RP).⁵³ The thinning of the retina induced by our implants in these pig studies approximates the retinal thickness that will be found in the human disease state. As such, the outcomes of these animal experiments informed our decisions about a preferred pillar height that likely will be appropriate, perhaps with some modification, for humans. The microfabrication methods used for these arrays could easily be modified to adjust the height of the posts to reach any desired location in the retina.

We will not know with certainty if our posts will penetrate the outer boundary of an end-stage human RP retina with the band of glial hypertrophy that develops in the outer retina in patients with RP, which Marc emphasized in his seminal histological studies.^{54,55} However, our intuition is that the posts will be able to penetrate the membrane given the substantial malleability of soft tissue when chronically opposed to a firmer object.

Our work in a large mammalian eye extends an initial observation of Palanker et al.³⁷ that penetrating electrodes could be positioned within the retina in much smaller rodent eyes. They also used an inactive array of pillars (10- μ m diameter; 65- μ m height) with variable center-to-center spacing.¹³ Later, Flores et al.⁵⁶ from the same group reported no visible gliosis in 90% of the implanted arrays (excluding two cases with gliosis from surgical trauma) in RCS rats, and like our work, variable height of pillars that could be designed to reach desired depths of the retinal architecture. Our use of larger eyes enabled testing of the device geometries, surgical tools, and surgical methods that are compatible for use in humans, and thus our model is well-suited for regulatory work needed to obtain US Food and Drug Administration approval for future implantation of a retinal prosthesis.

A weakness of this study is the relatively small number of surgical experiments that are reported, especially for the extraction studies. However, the

methods used herein represent the culmination of many years of evolution in our surgical methods, which began in rabbits and then progressed to a large number (>100) of surgeries in minipigs. Data reported in this manuscript represents a consecutive series of surgeries performed with methods and devices that derived from our most successful earlier experiments. Although our results confirm that our methods enable implantation of 3D arrays, the relatively low numbers, especially for the extractions, do not provide sufficient perspective about the consistency of being able to perform such maneuvers or the biological outcomes regarding cellular survival or gliosis. Thus our results should be received as being preliminary rather than definitive evidence in support of our conclusions. Our next step is to conduct additional procedures to improve the perspective of outcomes as part of preclinical implantations in minipigs toward the goal of achieving regulatory approval for human implants in the future.

Conclusions

Since these experiments were conducted, our team has produced electrically active 3D structures with similar geometries. These electrically active devices will be used in head-to-head experimental studies in animals and humans to validate the theoretical expectations of lower stimulation thresholds with penetrating versus planar electrodes. In addition to improved biocompatibility and survivability of electrodes, the anticipated lower stimulation charge levels needed to induce perception should confine the electrical fields to a relatively small cluster of neurons, which theoretically should provide more spatially detailed vision compared with prosthetics with planar electrodes.

Acknowledgments

The authors thank Alison Hayward, DVM, Arthur Nedder, DVM, and Diane Ghera of the animal care facilities at the Massachusetts Institute of Technology and the VA Boston Health Care System, Jamaica Plain for their assistance with the surgeries and postoperative animal care.

Supported by the Department of Veterans Affairs and the Massachusetts Lions Club.

Disclosure: **J. Chen**, Bionic Eye Technologies, Inc. (I); **V. Poulaki**, None; **S.-J. Kim**, None; **W.D. Eldred**, None; **S. Kane**, None; **M. Gingerich**, Bionic Eye

Technologies, Inc. (I,E,P); **D.B. Shire**, Bionic Eye Technologies, Inc. (I,E,P); **R. Jensen**, None; **G. DeWalt**, None; **H.J. Kaplan**, None; **J.F. Rizzo III**, Bionic Eye Technologies, Inc. (I,C,P,S)

References

- Alteheld N, Roessler G, Walter P. Towards the bionic eye—the retina implant: surgical, ophthalmological and histopathological perspectives. *Acta Neurochir Suppl.* 2007;97:487–493.
- Loewenstein JI, Montezuma SR, Rizzo JF, 3rd. Outer retinal degeneration: an electronic retinal prosthesis as a treatment strategy. *Arch Ophthalmol.* 2004;122:587–596. doi:10.1001/archophth.122.4.587.
- Winter JO, Cogan SF, Rizzo JF, 3rd. Retinal prostheses: current challenges and future outlook. *J Biomater Sci Polym Ed.* 2007;18:1031–1055. doi:10.1163/156856207781494403.
- Ganesan K, Stacey A, Meffin H, et al. Diamond penetrating electrode array for epi-retinal prosthesis. *Conf Proc IEEE Eng Med Biol Soc.* 2010;2010:6757–6760. doi:10.1109/IEMBS.2010.5626003.
- Humayun MS, Dorn JD, da Cruz L, et al. Interim results from the international trial of Second Sight's visual prosthesis. *Ophthalmology.* 2012;119:779–788. doi:10.1016/j.ophtha.2011.09.028.
- Rizzo JF, 3rd, Wyatt J, Loewenstein J, Kelly S, Shire D. Methods and perceptual thresholds for short-term electrical stimulation of human retina with microelectrode arrays. *Invest Ophthalmol Vis Sci.* 2003;44:5355–5361.
- Menzel-Severing JJ. Implantation and explantation of an active epiretinal visual prosthesis: 2-year follow-up data from the EPIRET3 prospective clinical trial. *Eye.* 26:501–509.
- Chen J, Shah HA, Herbert C, Loewenstein JI, Rizzo JF, 3rd. Extraction of a chronically implanted, microfabricated, subretinal electrode array. *Ophthalmic Res.* 2009;42:128–137. doi:10.1159/000227278000227278.
- Rizzo JF, 3rd, Shire DB, Kelly SK, et al. Overview of the boston retinal prosthesis: challenges and opportunities to restore useful vision to the blind. *Conf Proc IEEE Eng Med Biol Soc.* 2011;2011:7492–7495. doi:10.1109/IEMBS.2011.6093610.
- Rizzo JF, 3rd, Shire DB, Kelly SK, et al. Development of the boston retinal prosthesis. *Conf Proc IEEE Eng Med Biol Soc.* 2011;2011:3135–3138. doi:10.1109/IEMBS.2011.6090855.
- Sachs HG, Schanze T, Brunner U, Sailer H, Wiesnack C. Transscleral implantation and neurophysiological testing of subretinal polyimide film electrodes in the domestic pig in visual prosthesis development. *J Neural Eng.* 2005;2:S57–S64. doi:10.1088/1741-2560/2/1/008.
- Shire DB, Ellersick W, Kelly SK, et al. ASIC design and data communications for the Boston retinal prosthesis. *Conf Proc IEEE Eng Med Biol Soc.* 2012;2012:292–295. doi:10.1109/EMBC.2012.6345927.
- Butterwick A, Huie P, Jones BW, Marc RE, Marmor M, Palanker D. Effect of shape and coating of a subretinal prosthesis on its integration with the retina. *Exp Eye Res.* 2009;88:22–29. doi:10.1016/j.exer.2008.09.018.
- Mathieson K, Loudin J, Goetz G, et al. Photovoltaic Retinal Prosthesis with High Pixel Density. *Nat Photonics.* 2012;6:391–397. doi:10.1038/nphoton.2012.104.
- Wilke R, Gabel VP, Sachs H, et al. Spatial resolution and perception of patterns mediated by a subretinal 16-electrode array in patients blinded by hereditary retinal dystrophies. *Invest Ophthalmol Vis Sci.* 2011;52:5995–6003. doi:10.1167/iov.10-6946.
- Cai C, Li L, Li X, et al. Response properties of electrically evoked potential elicited by multi-channel penetrative optic nerve stimulation in rabbits. *Doc Ophthalmol.* 2009;118:191–204. doi:10.1007/s10633-008-9157-2.
- Gekeler K, Bartz-Schmidt KU, Sachs H, et al. Implantation, removal and replacement of subretinal electronic implants for restoration of vision in patients with retinitis pigmentosa. *Curr Opin Ophthalmol.* 2018;29:239–247. doi:10.1097/ICU.0000000000000467.
- Siu TL, Morley JW. In vivo evaluation of an episcleral multielectrode array for stimulation of the retina with reduced retinal ganglion cell mass. *J Clin Neurosci.* 2008;15:552–558. doi:10.1016/j.jocn.2007.06.012.
- Lane FJ, Huyck MH, Troyk P. Looking ahead: planning for the first human intracortical visual prosthesis by using pilot data from focus groups of potential users. *Disabil Rehabil Assist Technol.* 2011;6:139–147. doi:10.3109/17483107.2010.514381.
- Normann RA, Greger B, House P, Romero SF, Pelayo F, Fernandez E. Toward the development

- of a cortically based visual neuroprosthesis. *J Neural Eng.* 2009;6:035001. doi:10.1088/1741-2560/6/3/035001.
21. Srivastava NR, Troyk PR, Dagnelie G. Detection, eye-hand coordination and virtual mobility performance in simulated vision for a cortical visual prosthesis device. *J Neural Eng.* 2009;6:035008. doi:10.1088/1741-2560/6/3/035008.
 22. Tani N, Hirata M, Motoki Y, et al. Quantitative analysis of phosphenes induced by navigation-guided repetitive transcranial magnetic stimulation. *Brain Stimul.* 2011;4:28–37. doi:10.1016/j.brs.2010.03.006.
 23. Lewis Philip MP. Restoration of vision in blind individuals using bionic devices: a review with a focus on cortical visual prostheses. *Brain Research.* 2015;1595:51–73.
 24. Torab K, Davis TS, Warren DJ, House PA, Normann RA, Greger B. Multiple factors may influence the performance of a visual prosthesis based on intracortical microstimulation: nonhuman primate behavioural experimentation. *J Neural Eng.* 2011;8:035001. doi:10.1088/1741-2560/8/3/035001.
 25. Troyk PR, Bradley D, Bak M, et al. Intracortical visual prosthesis research - approach and progress. *Conf Proc IEEE Eng Med Biol Soc.* 2005;7:7376–7379. doi:10.1109/IEMBS.2005.1616216.
 26. Abramian M, Dokos S, Morley JW, Lovell NH. Activation of ganglion cell axons following epiretinal electrical stimulation with hexagonal electrodes. *Conf Proc IEEE Eng Med Biol Soc.* 2010;2010:6753–6756. doi:10.1109/IEMBS.2010.5626002.
 27. Jensen RJ. Activation of ganglion cells in wild-type and P23H rat retinas with a small subretinal electrode. *Exp Eye Res.* 2012;99:71–77. doi:10.1016/j.exer.2012.03.016.
 28. Jensen RJ, Rizzo JF, 3rd. Thresholds for activation of rabbit retinal ganglion cells with a subretinal electrode. *Exp Eye Res.* 2006;83:367–373. doi:10.1016/j.exer.2006.01.012.
 29. Johnson L, Perkins FK, O’Hearn T, et al. Electrical stimulation of isolated retina with microwire glass electrodes. *J Neurosci Methods.* 2004;137:265–273. doi:10.1016/j.jneumeth.2004.02.035.
 30. Kasi H, Hasenkamp W, Cosendai G, Bertsch A, Renaud P. Simulation of epiretinal prostheses – evaluation of geometrical factors affecting stimulation thresholds. *J Neuroeng Rehabil.* 2011;8:44 doi:10.1186/1743-0003-8-44.
 31. Sekirnjak C, Hottowy P, Sher A, Dabrowski W, Litke AM, Chichilnisky EJ. High-resolution electrical stimulation of primate retina for epiretinal implant design. *J Neurosci.* 2008;28:4446–4456. doi:10.1523/JNEUROSCI.5138-07.2008.
 32. Fried S, Jensen RJ. The Response of Retinal Neurons to Electrical Stimulation: A Summary of in-vitro and in-vivo Animal Studies. In: Dagnelie G, ed. *Visual Prosthetics: Physiology, Bioengineering, Rehabilitation*: Springer, 2011:229–258.
 33. Jensen RJ, Ziv OR, Rizzo JF, 3rd. Thresholds for activation of rabbit retinal ganglion cells with relatively large, extracellular microelectrodes. *Invest Ophthalmol Vis Sci.* 2005;46:1486–1496. doi:10.1167/iovs.04-1018.
 34. Schmidt EM, Bak MJ, Hambrecht FT, Kufta CV, O’Rourke DK, Vallabhanath P. Feasibility of a visual prosthesis for the blind based on intracortical microstimulation of the visual cortex. *Brain.* 1996;119:507–522.
 35. Sun J, Lu Y, Cao P, et al. Spatiotemporal properties of multip peaked electrically evoked potentials elicited by penetrative optic nerve stimulation in rabbits. *Invest Ophthalmol Vis Sci.* 2011;52:146–154. doi:10.1167/iovs.09-4024.
 36. Normann RA, Maynard EM, Rousche PJ, Warren DJ. A neural interface for a cortical vision prosthesis. *Vision Res.* 1999;39:2577–2587.
 37. Palanker D, Vankov A, Huie P, Baccus S. Design of a high-resolution optoelectronic retinal prosthesis. *J Neural Eng.* 2005;2:S105–S120. doi:10.1088/1741-2560/2/1/012.
 38. Nguyen HT, Tangutooru SM, Rountree CM, et al. Thalamic visual prosthesis. *IEEE Trans Biomed Eng.* 2016;63:1573–1580. doi:10.1109/TBME.2016.2567300.
 39. Jensen RJ, Rizzo JF, 3rd, Ziv OR, Grumet A, Wyatt J. Thresholds for activation of rabbit retinal ganglion cells with an ultrafine, extracellular microelectrode. *Invest Ophthalmol Vis Sci.* 2003;44:3533–3543.
 40. Palanker DHP, Vankov A, Aramant R, Seiler M, Fishman H, Marmor M, Blumenkranz M. Migration of retinal cells through a perforated membrane: implications for a high-resolution prosthesis. *Invest Ophthalmol Vis Sci.* 2004;45(Sep):3266–3270.
 41. Chen JL, Kim SJ, Memon MA, Snebold LS, Masrur F, Gingerich MD, Shire DB, Rizzo JF. *Surgical implantation of different geometries of electrode arrays in minipig eyes.* Association for Research in Vision and Ophthalmology Florida, 2008.
 42. Montezuma SR, Loewenstein J, Scholz C, Rizzo JF, 3rd. Biocompatibility of materials implanted into the subretinal space of Yucatan pigs. *Invest*

- Ophthalmol Vis Sci.* 2006;47:3514–3522. doi:10.1167/iovs.06-0106.
43. Kane SR, Ashby PD, Pruitt LA. Microscale wear behavior and crosslinking of PEG-like coatings for total hip replacements. *J Mater Sci Mater Med.* 2010;21:1037–1445. doi:10.1007/s10856-009-3935-6.
 44. Traverso V, Kinkl N, Grimm L, Sahel J, Hicks D. Basic fibroblast and epidermal growth factors stimulate survival in adult porcine photoreceptor cell cultures. *Invest Ophthalmol Vis Sci.* 2003;44:4550–4558. doi:10.1167/iovs.03-0460.
 45. Boinagrov D, Pangratz-Fuehrer S, Goetz G, Palanker D. Selectivity of direct and network-mediated stimulation of the retinal ganglion cells with epi-, sub- and intraretinal electrodes. *J Neural Eng.* 2014;11:026008. doi:10.1088/1741-2560/11/2/026008.
 46. Loudin JD SD, Vijayraghavan K, Sramek CK, Butterwick AF, Huie P, McLean GY, Palanker DV. Optoelectronic retinal prosthesis: system design and performance. *J Neural Eng.* 2007;4:S72–S84.
 47. Cogan SF. Neural stimulation and recording electrodes. *Annu Rev Biomed Eng.* 2008;10:275–309. doi:10.1146/annurev.bioeng.10.061807.160518.
 48. Cogan SF, Ludwig KA, Welle CG, Takmakov P. Tissue damage thresholds during therapeutic electrical stimulation. *J Neural Eng.* 2016;13:021001. doi:10.1088/1741-2560/13/2/021001.
 49. Cogan SF, Plante TD, Ehrlich J. Sputtered iridium oxide films (SIROFs) for low-impedance neural stimulation and recording electrodes. *Conf Proc IEEE Eng Med Biol Soc.* 2004;6:4153–4156. doi:10.1109/IEMBS.2004.1404158.
 50. McCreery D, Pikov V, Troyk PR. Neuronal loss due to prolonged controlled-current stimulation with chronically implanted microelectrodes in the cat cerebral cortex. *J Neural Eng.* 2010;7:036005. doi:10.1088/1741-2560/7/3/036005.
 51. Shannon RV. A model of safe levels for electrical stimulation. *IEEE Trans Biomed Eng.* 1992;39:424–426. doi:10.1109/10.126616.
 52. Schmidt EM, Bak MJ, Hambrecht FT, Kufta CV, O'Rourke DK, Vallabhanath P. Feasibility of a visual prosthesis for the blind based on intracortical microstimulation of the visual cortex. *Brain.* 1996;119:507–522.
 53. Jones BW, Pfeiffer RL, Ferrell WD, Watt CB, Marmor M, Marc RE. Retinal remodeling in human retinitis pigmentosa. *Exp Eye Res.* 2016;150:149–165. doi:10.1016/j.exer.2016.03.018.
 54. Marc RE, Jones BW. Retinal remodeling in inherited photoreceptor degenerations. *Mol Neurobiol.* 2003;28:139–147. doi:10.1385/MN:28:2:139.
 55. Marc RE, Jones BW, Watt CB, Strettoi E. Neural remodeling in retinal degeneration. *Prog Retin Eye Res.* 2003;22:607–655.
 56. Flores TA, Lei X, Huang TW, et al. Optimization of pillar electrodes in subretinal prosthesis for enhanced proximity to target neurons. *J Neural Eng.* 2018. doi:10.1088/1741-2552/aac39.